Electronic Supplementary Material (ESI) for CrystEngComm.

Supporting Information

Facile and green synthesis of decatungstate-based nickle(II) complex coated modified-Fe_3O_4 nanoparticles with enhanced antibiotic-resistant activity

Cuili Xing, Pengtao Ma, Meng Zhao, Jiangnan Chang, Xiaoyuan Guo, Lin Sun*and Mingxue Li*

Henan Key Laboratory of Polyoxometalates, Institute of Molecular and Crystal Engineering, College of Chemistry and Chemical Engineering, Henan University, Kaifeng 475004, P. R. China

E-mail: sunlin@vip.henu.edu.cn (L. Sun); limingxue@henu.edu.cn (M. Li).

1. Experimental Section

1.1 Materials and Characterization

All chemicals and reagents used in this work were analytical grade and received no further purification. Iron(III) chloride hexahydrate ($FeCl_3 \cdot 6H_2O$, 99%), ferrous chloride tetrahydrate ($FeCl_2$ $4H_2O$, 98%), tris(hydroxymethyl) aminomethane (Tris, 99.9%), dopamine hydrochloride (98%), sodium molybdate dehydrate ($Na_2WO_4 \cdot 2H_2O$, 99%), nickelous perchlorate hexahydrate ($Ni(ClO_4)_2 \cdot 6H_2O$, 99%) and phenylphosphonic acid ($C_6H_5PO_3H_2$, 99%) were purchased from J&K Scientific Ltd. (Beijing, China). Sodium chloride (NaCl, 99.5%), sodium hydroxide (NaOH, 96%), hydrochloric acid (HCl, 36-38%), and ethanol (CH_3CH_2OH, 99.7%) were obtained from Aldrich (Shanghai, China). Sterile filtration membranes (0.22 μm) used for filtering large particles, were bought from Millipore.

Powder X-ray diffractometer (Philips X'Pert Pro, Philips, Amsterdam, Netherlands) equipped with Cu *K*α radiation (λ = 1.54056Å) were used to investigate the crystallized property. The morphology and microstructures were observed by a field emission scanning electron microscope (FESEM, Zeiss supra55) and transmission electron microscopy (TEM, FEI Tencnai G2F30). X-ray photoelectron spectroscopy were obtained using a Thermo ESCALAB 250XI photoelectron spectrometer (ThermoFisher Scientific, Waltham, MA, USA) with Al *K*α X-ray (hv = 1486.6 eV) as the excitation resource. Fourier transform infrared (FT-IR) spectra were recorded using a Bruker AVATEX-70 Fourier infrared spectrometer with an operating range of 400–4000 cm^{-1}. Elemental analyses were carried out on a Flash 2000 analyzer (Elementar, Hessia, Germany). The room temperature hysteresis loops of the products were measured using a vibrating sample magnetometer (VSM, Lakeshore 7300, USA). The morphology changes of bacteria were monitored using SEM micrographs (Gemini 500).

1.2 Integrity of bacterial cell membrane of *E. coli*

At first, 4 mg Fe_3O_4@PDA@Ni-DT composite was added into 4 mL of bacterial cell suspension to form a mixture, which was incubated at 37 °C for 15 min in

thermostatic incubator. Afterward, the solution was filtered through 0.22 μm syringe filters, and the filtrate was detected by UV-vis spectrophotometer to determine the absorbance changes with a maximum absorption wavelength of 260 nm.

Firstly, *E. coli* bacterial suspension and Fe_3O_4@PDA@Ni-DT composites were incubated at 37 °C for 1 h in thermostatic incubator. Then, 1.0 mL of the treated bacterial suspensions was taken out and transferred into EP tube every 15 min, and 5 mL coomassie brilliant blue solution was added into the EP tube. After that the mixture was shaken well and reacted for 2 min. Finally, the absorbance of the mixed solution was measured at 595 nm.

1.3 Enzymatic activity of *E. coli*

The *E. coli* cells boiled for 20 min were inactivated completely as the negative control (–), the bacterial cells no boiled and maintained native activity of enzymes as the positive control (+). INT solution (0.5%, 0.1 mL) was added into the bacterial cells and treated with Fe_3O_4@PDA@Ni-DT composites (1 $mg \cdot mL^{-1}$). The mixed solution was incubated at 37 °C for 15 min in dark condition. Then the reaction was terminated by adding 50 μL of formaldehyde. The mixture was centrifuged to collect the bacteria, and 250 μL solutions of acetone and ethanol by 1:1 in volume were used to distill the INF for twice time. Finally, the obtained supernatants were mixed and the absorbance of INF was measured at 490 nm.

1.4 Oxidative stress mediated by Fe_3O_4@PDA@Ni-DT composites

Firstly, 1.0 mL bacterial suspension with 4 mg Fe_3O_4@PDA@Ni-DT composites was cultured for 15 min at 37 °C in thermostatic incubator. Then 4.0 mL (1 $mg \cdot mL^{-1}$) NBT solution was added and cultured for 30 min at 37 °C in thermostatic incubator. Afterwards 0.4 mL HCl (0.1 M) was added to stop the reaction. Then, the reacted suspensions were centrifuged for 10 min at 5000 rpm to remove the supernatants. After that, the collected bacterial cells were treated with 1.0 mL of dimethyl sulfoxide (DMSO) to extract the reduced NBT and the extracted solution was diluted. Finally, the absorbance of diluted extraction solution was measured at 575 nm.

In vitro GSH oxidation is used as an oxidative stress indicator because thiol groups (–SH) in GSH can be oxidized to disulfide bond (–S–S–), which converts GSH

to glutathione disulfide (GSSG). Bicarbonate buffer (pH = 8.6) was used as reaction solution and all samples were prepared in triplicate. Pure GSH solution was used as negative control (–) and GSH solution with H_2O_2 (1 mM) as positive control (+).4.0 mg Fe_3O_4@PDA@Ni-DTs was added into 1 mL of GSH (0.8 mM) to initiate oxidation. Then all the mixtures were placed in a shaker with a speed of 150 rpm for 2 h in dark. After incubation, 3.5 mL of 0.05 M Tris-HCl and 70 μL of 5, 5-dithiobis-(2-nitrobenzoic acid) (DTNB) were added into the mixtures to yield yellow product. The mixtures were filtrated through 0.22 μm syringe filters. Measurements of the thiol content with all samples were carried out at 412 nm. The loss of GSH was calculated by the following formula: loss of GSH % = $(OD_{control\ (-)} - OD_{sample})/OD_{control\ (-)} \times 100\%$.

2. Characterization

2.1 Structural description of Ni-DT crystal

The molecule structure of complex $[Ni(HL)_2]_2[W_{10}O_{32}]\cdot 4H_2O$ (**Figure S1a**) was composed of two $[Ni(HL)_2]^{2+}$ cations, a $[W_{10}O_{32}]^{4-}$ anion and four lattice water molecules. N4 and S1 atoms were located in axial position, while N3, N8, N7 and S2 atoms were situated in equatorial position. The dihedral angles between chelate rings (Ni1–N4–C4–C2–N3)···(Ni1–S1–C1–N2–N3) and (Ni1–N8–C12–C10–N7)···(Ni1–S2–C9–N6–N7) were approximately 8.766 and 2.526°, respectively. The distance of Ni1–N was 2.002–2.121 Å and Ni1–S was 2.429–2.440 Å. The range of angles N–Ni1–N and N–Ni1–S was 77.2 (4)–173.8 (4)° and 81.7 (3)–159.5(3)°. In the $\{W_5O_{18}\}$ unit, five distorted $\{WO_6\}$ octahedra were connected by one common oxygen atom co-edge, and two $\{W_5O_{18}\}$ units were formed by four common oxygen atom co-angle junctions $[W_{10}O_{32}]^{4-}$ anion. Seven hydrogen bonds N6–H6A···O1W, N2–H2A···O5, N1–H1B···O10, N5–H5A···O1W, N1–H1A···O8, N5–H5B···O9, N1–H1A···O9 interactions exist in complex $[Ni(HL)_2]_2[W_{10}O_{32}]$. Finally, the $[W_{10}O_{32}]^{4-}$ and $[Ni(HL)_2]^{2+}$ units as well as water molecules could form a 2D structural stacking map by hydrogen bonding to each other (**Figure S1b**).

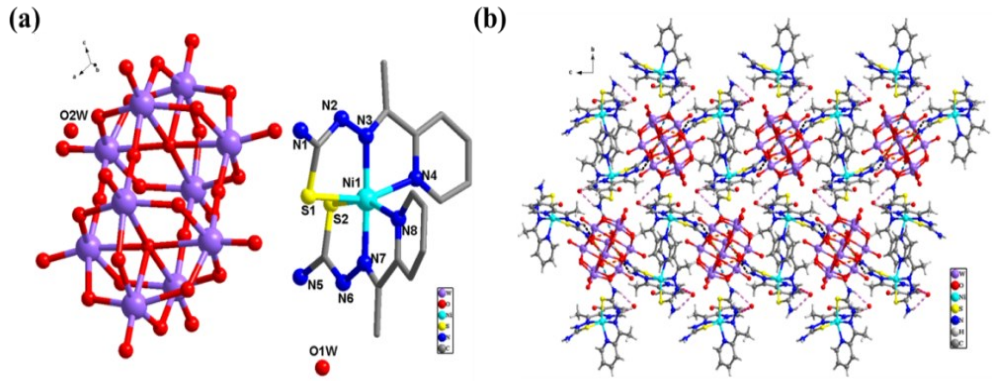

Figure S1. (a) The molecule structure of Ni-DT; (b) $[W_{10}O_{32}]^{4-}$, $[Ni(HL)_2]^{2+}$ and two-dimensional structural stacking maps formed by hydrogen bonding between water molecules

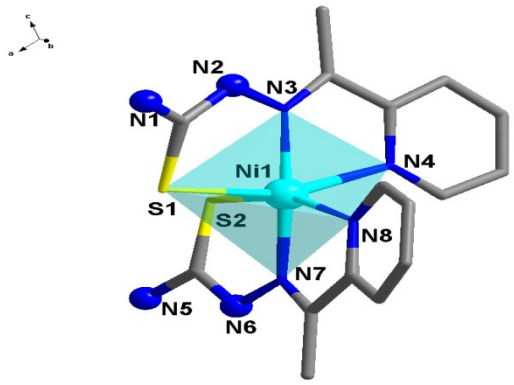

Figure S2. Octahedral geometry of $[Ni(HL)_2]^{2+}$

2.2 IR spectra and PXRD analysis

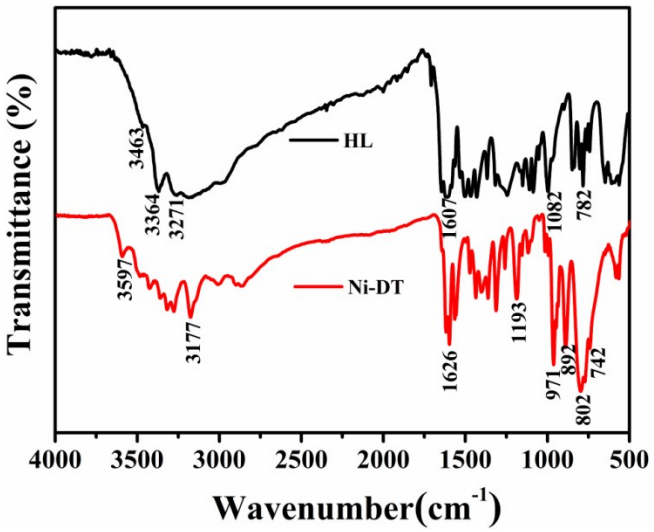

Figure S3. IR spectra of Ni-DT

The IR spectra (**Figure S3**) of prepared Ni-DT shows characteristic bands of the $[W_{10}O_{32}]^{4-}$ polyoxoanion at 971 cm^{-1}, 892 cm^{-1} and 802 cm^{-1}. The peak at 971 cm^{-1}

corresponds to the vibration of the terminal W=O bond. The absorption bands in the range 500–892 cm^{-1} correspond to the vibrations of different type bridging W–O–W groups.[1] The absorption bands in the range 1000-3600 cm^{-1} correspond to absorption of the $[Ni(HL)_2]^{2+}$ cation and crystallization water, which is consistent with the literature data.[2–4] In a word, these results of IR spectrum are well consistent with those of X-ray diffraction structural analysis. PXRD spectra of as-prepared Ni-DT match well with the simulated pattern (**Figure S4**).

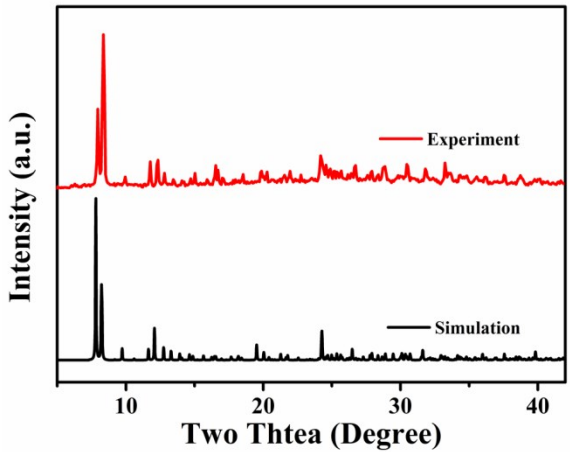

Figure S4. PXRD pattern of Ni-DT

2.3 TG analysis

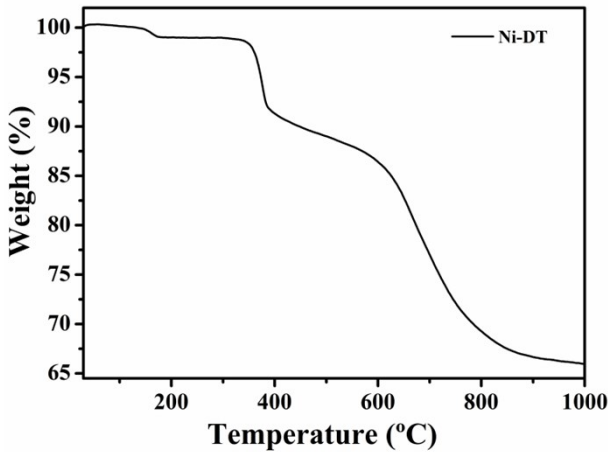

Figure S5. The TGA curve of Ni-DT

TGA was performed to observe the thermal stability of Ni-DT in a flowing N_2 atmosphere at 30–1000 °C and a heating rate of 10 °C·min^{-1} (Figure S5). The TGA curve of Ni-DT indicates a two-step weight-loss process. The first weight loss of 1.03% (cacld, 2.17%) below 200 °C was assigned to the loss of lattice water molecules, in which the difference in practical and theoretical values may be due to a small amount

of water loss and weathering. The second weight loss was ascribed to the removal of four ligands and the decomposition of the POM anion skeleton.[5–7] The framework of Ni-DT was stable up to 300 ºC. The high thermal stability afforded an ideal prerequisite for pharmacological application.

Table S1. Crystal data and structure refinement results for Ni-DT

Crystal Data	**Ni-DT**
Empirical formula	$C_{32}H_{40}Ni_2W_{10}N_{16}O_{36}S_4$
Formula weight	3308.96
Crystal system	Monoclinic
Space group	P2(1)/c
T (K)	296(2)
a (Å)	11.3341(11)
b (Å)	21.413(2)
c (Å)	14.0095(13)
α (deg)	90.00
β (deg)	108.101(2)
γ (deg)	90.00
V (Å^3)	3231.9(5)
Z	2
Dc (g cm^{-3})	3.400
μ (mm^{-1})	18.512
θ (deg)	1.89–25.00
F(000)	2984.0
Independent reflections	5683 [R_{int} = 0.0544, R_{sigma} = 0.0652]
Data/restraints/parameters	5683/72/436
R_1[a], wR_2[b] [$I \geq 2\sigma$ (I)]	0.0388, 0.0993
R_1, wR_2, (all data)	0.0478, 0.1033
diff peak and hole, eÅ^{-3}	2.983/–1.937

Table S2. Selected Bond Distances (Å) and angles (°) for Ni-DT

Ni-DT			
Ni(1)–S(2)	2.428(3)	W(1)–O(3)	1.700(7)
Ni(1)–S(1)	2.442(3)	W(1)–O(4)	1.890(7)
Ni(1)–N(7)	2.016(8)	W(1)–O(6)	1.913(7)
Ni(1)–N(3)	2.015(8)	W(1)–O(1)	1.911(7)
Ni(1)–N(8)	2.082(8)	W(1)–O(5)	1.941(7)
Ni(1)–N(4)	2.115(9)	W(1)–O(2)	2.290(6)
W(2)–O(7)	1.725(7)	W(3)–O(9)	1.699(7)
W(2)–O(8)	1.879(7)	W(3)–O(11)	1.833(6)
W(2)–O(15)	1.916(6)	W(3)–O(10)	1.928(6)
W(2)–O(6)	1.939(7)	W(3)–O(5)	1.936(6)
W(2)–O(13)	1.978(7)	W(3)–O(8)	2.026(7)
W(2)–O(2)	2.290(6)	W(3)–O(2)	2.286(6)
N7–Ni1–N3	173.9(3)	N8–Ni1–S2	159.7(3)

N7–Ni1–N8	77.5(3)	N4–Ni1–S2	88.4(2)
N3–Ni1–N8	99.3(3)	N7–Ni1–S1	92.9(3)
N7–Ni1–N4	108.1(3)	N3–Ni1–S1	81.8(3)
N3–Ni1–N4	77.2(3)	N8–Ni1–S1	88.7(3)
N8–Ni1–N4	95.2(3)	N4–Ni1–S1	159.0(2)
N7–Ni1–S2	82.4(3)	S2–Ni1–S1	95.06(11)
N3–Ni1–S2	100.9(2)		

2.4 SEM and EDX images

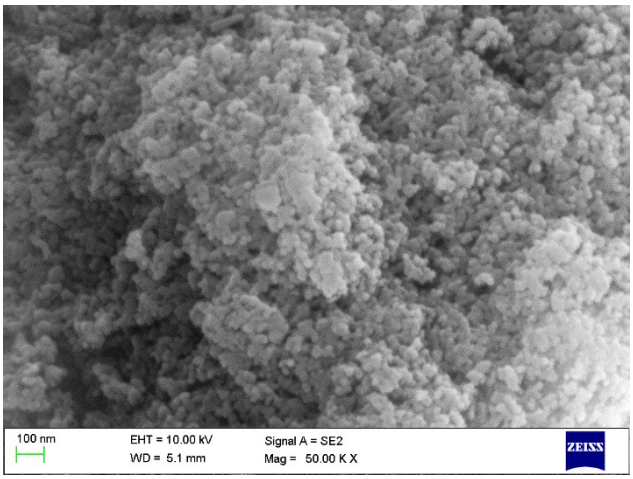

Figure S6. SEM image of the Fe_3O_4@PDA@Ni-DT composites

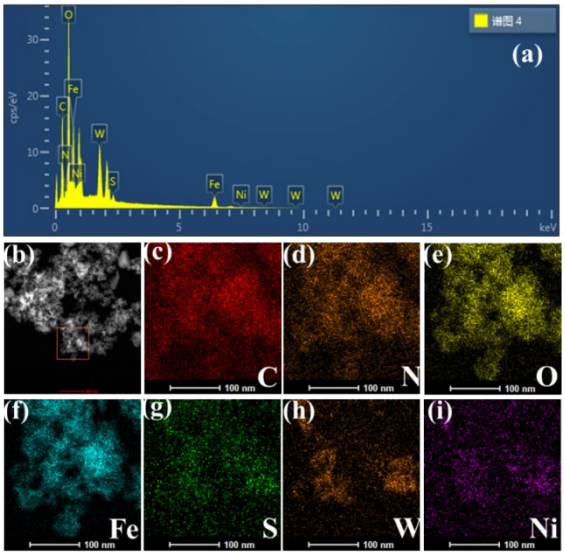

Figure S7. (a) EDX images of the prepared nanostructured Fe_3O_4@PDA@Ni-DT composites (b) HAADF-STEM image and (c–i) the corresponding HAADF-STEM-EDS elemental mappings of the prepared sample

2.5 Antibacterial activity

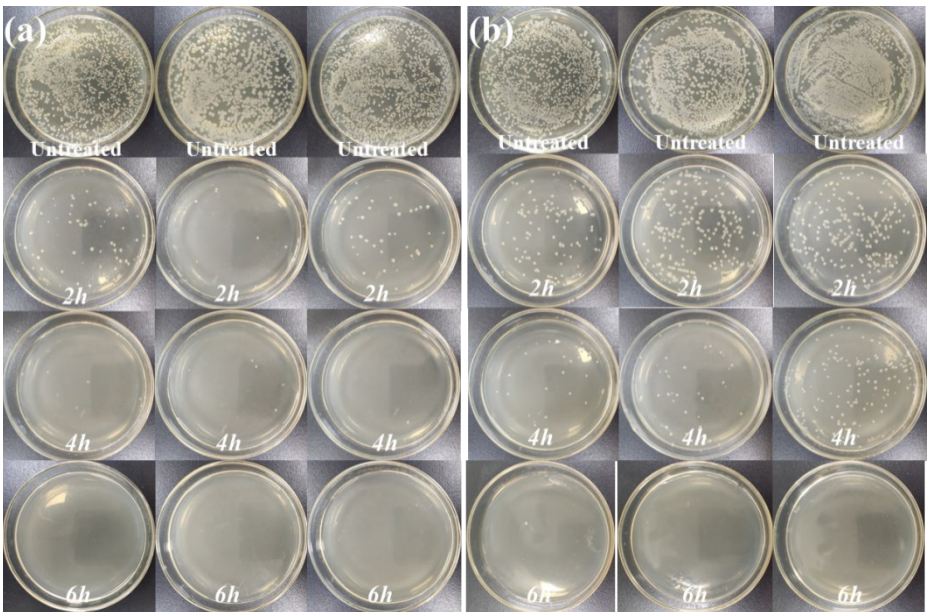

Figure S8. The optical photographs of Fe_3O_4@PDA@Ni-DT at different time interviel against (a) *28a* and (b) *22b*

Table S3 Summary and comparison of similar materials on antibacterial activity

Nanocomposites	**Surface modifier**[a]	**proposed antibacterial approach**	**experimental microbe**	Antibacterial effects	**Ref.**
IONPs@pDA-Nisin	Nisin	contact killing of Nisin	Alicyclobacillus acidoterrestris	72%	8
Fe_3O_4@PDA@Ru-NO@FA	Ru-NO@FA	photothermal killing	*E. coli, S. aureus*	-	9
Fe_3O_4@PDA@HL	Schiff base ligand	contact killing of HL	*E. coli, S. aureus*	-	10
Fe_3O_4@PDA@PAMAM@NONOate	PAMAM@NONOate	synergistic photothermal and NO treatment	*E. coli, S. aureus*	Almost 100%	11
Fe_3O_4@PDA@POM	Cu-POM	contact killing of POM	*E. coli, S. aureus*	99.9%	12
Fe_3O_4-PDA-Ag	Ag	contact killing of Ag	*E. coli, S. aureus*	100%	13
Fe_3O_4@PDA@Ni-DT	Ni-DT	contact killing of Ni-DT	*E. coli, S. aureus* and two antibiotic resistant bacteria	Almost 100%	This paper

[a] [8] IONPs = iron oxide nanoparticles; [9] ruthenium nitrosyl (Ru-NO), NO = nitric oxide, FA = folic acid; [10] HL = 3-aminopyridine-2-carboxaldehyde N(4)-methylthiosemicarbazone; [11] PAMAM = poly(amidoamine), N-diazeniumdiolate = NONOate; [12] Cu-POM = $[Cu(HL)_4]_2[P_2Mo_5O_{23}]_2 \cdot 8H_2O$ (L = 2-aminopyridine), [13] HL = 2-acetylpyridine thiosemicarbazone

Table S4 The control antibacterial studies against two antibiotic resistant bacteria *E. coli*, Ni^{2+}, HL and $W_{10}O_{32}^{4-}$ were assayed as the control

	Sample name			
	Ni^{2+} [a]	HL	$W_{10}O_{32}^{4-}$ [b]	Ni-DT
Amounts (μmol)	0.5	2.6	0.7	0.5
28a	50.0%	28.17%	51.29%	73.21%
22b	55.67%	20.63%	44.77%	68.95%

[a] Ni^{2+} derived from $Ni(ClO_4)_2 \cdot 6H_2O$ (M=365.70 g mol^{-1}); [b] $[W_{10}O_{32}]^{4-}$ derived from $[(n\text{-}C_4H_9)_4N]_4[W_{10}O_{32}]$ (M=2742.40 g mol^{-1})

3. Notes and references

[1] N. V. Kuratieva, S. P. Khranenko, S. A. Gromilov, *J. Struct. Chem.,* 2014, **55**, 285–289.

[2] Y. Fang, Y. T. Wang, M. Zhao, Y. L. Lu, M. X. Li, Y. H. Zhang, *Polyhedron*, 2018, **155**, 254–260.

[3] R. K. Singh, A.K. Singh, *J. Mol. Struct.,* 2015, **1094**, 61–72.

[4] J. Li, H. Y. Zhao, C. G. Ma, Q. X. Han, M. X. Li, H. L. Liu, *Nanomaterials,* 2019, **9**, 649.

[5] J. Li, B. W. Chang, H.Y. Zhao, Q. X. Meng, M. X. Li, Q. X. Han, J. Mater. Sci., 2021, **56**, 6676–6688.

[6] D. Wang, L.L. Liu, J. Jiang, L.J. Chen, J.W. Zhao, *Nanoscale* 2020, **12**, 5705–5718.

[7] J. Li, J. C. He, C. Si, M. X. Li, Q. X. Han, Z. L. Wang, J. W. Zhao, *J. Catal.,* 2020, **392**, 244–253.

[8] Z. H. Song, C. Niu, H. Wu, J. P. Wei, Y. X. Zhang, T. L. Yue, *ACS Appl. Mater. Interfaces* 2019, **11**, 21874–21886.

[9] Y. T. Yu, S. W. Shi, Y. Wang, Q. L. Zhang, S, H. Gao, S.P. Yang, J. G. Liu, *ACS Appl. Mater. Interfaces* 2020, **12**, 312−321.

[10] Y. Fang, C. L. Xing, S. X. Zhan, M. Zhao, M. X. Li, H. L. Liu, C.Z. Wang, *ACS Biomater. Sci. Eng.*, 2019, **5**, 6779−6793.

[11] S.M. Yu, G. W. Li, R. Liu, D. Ma, W. Xue, *Adv. Funct. Mater.*, 2018, 1707440.

[12] Y. Fang, C. L. Xing, S. X. Zhan, M. Zhao, M. X. Li, H. L. Liu, *J. Mater. Chem. B*, 2019, **7**, 1933−1944.

[13] P. Qin, C. Chen, Y. B. Wang, L. T. Zhang, P. Wang, *J. Nanosci. Nanotechnol.*, 2017, **17**, 9350–9355.